

# ECAFormer: Low-light Image Enhancement using Cross Attention

Yudi Ruan, Hao Ma, Weikai Li\* and Xiao Wang\*, *Senior Member, IEEE*

**Abstract**— Low-light image enhancement (LLIE) is vital for autonomous driving. Despite the importance, existing LLIE methods often prioritize robustness in overall brightness adjustment, which can come at the expense of detail preservation. To overcome this limitation, we propose the Hierarchical Mutual Enhancement via Cross-Attention transformer (ECAFormer), a novel network that utilizes Dual Multi-head Self Attention (DMSA) to enhance both visual and semantic features across scales, significantly preserving details during the process. The cross-attention mechanism in ECAFormer not only improves upon traditional enhancement techniques but also excels in maintaining a balance between global brightness adjustment and local detail retention. Our extensive experimental validation on renowned low-illumination datasets, including SID and LOL, and additional tests on dark road scenarios, or performance over existing methods in terms of illumination enhancement and noise reduction, while also optimizing computational complexity and parameter count, further boosting SSIM and PSNR metrics. Our project is available at <https://github.com/ruanyudi/ECAFormer>.

**Index Terms**—Image Restoration, Cross Attention, Transformer, Feature fusion.

## I. INTRODUCTION

CAPTURING images in low-light conditions frequently leads to a variety of photographic challenges, such as the loss of fine details, a reduction in color intensity, a decrease in contrast and dynamic range, and uneven exposure. These issues can degrade the quality and clarity of the visual data, which in turn can significantly hinder subsequent vision-based tasks. For instance, they can impede the performance of autonomous driving systems [1]–[3], nighttime surveillance efforts [4], and remote sensing applications [5]. Enhancing the visibility of objects and details in low-light images is, therefore, a critical issue with broad implications for a range of applications.

To enhance the low-light images, numerous algorithms have been proposed to address the challenges encountered in low-light environments. These algorithms can be broadly categorized into two groups: knowledge-driven methods and data-driven methods.

Weikai Li and Xiao Wang are corresponding authors.

Yudi Ruan is with the School of Information Science and Engineering, Chongqing Jiaotong University, Chongqing, 400074, China (e-mail: yudi.ruan@mails.cqjtu.edu.cn).

Hao Ma is with the School of Artificial Intelligence, Anhui University, Hefei, Anhui, 230039, China (e-mail: WA22301107@stu.ahu.edu.cn).

Weikai Li is with the School of Mathematics and Statistics, Chongqing Jiaotong University, Chongqing, 400074, China, MIIT Key Laboratory of Pattern Analysis and Machine Intelligence, Nanjing, 210016, China (e-mail: leeweikai@outlook.com).

Xiao Wang is with School of Artificial Intelligence, Anhui University, Hefei, Anhui, 230039, China (e-mail: x.wang@atu.edu.cn).

Manuscript received April 19, 2021; revised August 16, 2021.

Knowledge-driven methods for low-light enhancement include Histogram Equalization-based methods [6], [7] and Retinex model-based methods [8]–[15]. Among these, the Retinex model-based methods have received relatively more attention. A typical Retinex model-based approach decomposes a low-light image into a reflection component and an illumination component using priors or regularizations. However, models based on theoretical principles often overlook factors present in the real environment due to the idealization of the theory, and thus may not produce satisfactory results.

Data-driven methods often use convolutional neural networks (CNNs) to learn complex image features and generate enhanced images based on these features. Typical examples include AutoEncoder (AE) [16], generative adversarial networks (GANs) [17]. These deep learning models are also divided into end-to-end models and theoretical prior-based models, while the latter use prior experience to constrain the neural network [18], [19]. Due to the defects in the ideal assumptions, prior-based methods may fall into bias. Compared to the explosive development of **Transformer models** in other fields, the potential of Transformer models in the LLIE field has not yet been fully tapped. Additionally, low-light image enhancement demands spatially varying operations [20], although transformers are particularly adept at capturing long-range information. While SNRNet [20] acknowledged this aspect, it solely relied on a single layer of global transformer, thereby overlooking the crucial interaction between information across varying hierarchical levels.

Regarding the current situation in the LLIE field, we proposed a transformer-based Network with an novel efficient fusion module, fully utilizing information from different scales to integrate the requirements of long-range and short-range. Meanwhile, the addition of pre-convolution compensates for the spatial context induction bias in transformers that rely solely on positional embeddings. Our main contribution can be summarized as follows:

- Our major idea is to comprehensively combine the local(short-range) detail feature extraction ability of CNN networks and the global(long-range) information interaction ability of Transformer networks, and utilize the multi-scale interaction ability of U-shaped networks to improve the processing ability of the Enhanced-network.
- We propose a advanced method called **ECAFormer** to simultaneously and effectively extract short-range and long-range features. **DMSA** blocks enable the network to have powerful feature fusion capabilities. Our work has made meaningful attempts and innovations in the development of transformer models in the field of LLIE.

- We validated our proposed method on six datasets, and extensive experimental results showed that our method has top-notch performance and good robustness at the same time. Meanwhile, our proposed network has a top-notch improvement effect at the same computational complexity.

The paper is structured as follows. In Chapter II, we respectively reviewed the related work in the field of low light enhancement and cross-attention mechanisms. In Chapter III, we introduced the definition of the problem, the proposed method, and the details of model optimization. In Chapter IV, we compared our model with seven publicly available datasets and conducted ablation experiments to validate its effectiveness. Finally, we summarized in Chapter V and proposed directions for future work.

## II. RELATED WORK

### A. LLIE: low light image enhancement

**Knowledge-driven methods.** CLAHE [21] normalizes the value of each pixel in an image based on a histogram function, which lacks local adaptability and can easily lead to overexposure or underexposure in images. Earlier works addressed this issue by optimizing the parameters in the equalization function, such as [22], which enhanced the adaptability of the method by altering one or two parameters using a generalization of histogram equalization. Subsequent extensive research has begun using priors to constrain the equalization process. Brightness Preserving Dynamic Histogram Equalization (BPDHE) [6] extends traditional Histogram Equalization (HE) by producing an output image whose mean intensity closely matches that of the input. This method effectively fulfills the requirement to maintain the original mean brightness of the image. [23] adjust the level of contrast enhancement by introducing specifically designed penalty terms through noise robustness, white/black stretching and mean-brightness preservation. The Retinex model [24] and its multi-scale variant [25] decompose brightness into illumination and reflectance components, which are then processed independently. LIME [11] introduced a structural prior to refine the initial illumination map, ultimately synthesizing the enhanced image in accordance with Retinex theory. Additionally, there are some works based on gamma correction, such as an adaptive gamma correction (AGC) [26] that is proposed to enhance the image contrast appropriately. The parameters of AGC are dynamically set based on the image information.

However, these manually crafted constraints and priors lack sufficient self-adaptivity to accurately recover image details and colors, often leading to the obliteration of details, local under- or over-saturation, uneven exposure, or the emergence of halo artifacts around objects. Given the demonstrated advantages of deep learning across various low-level visual tasks, the field of low-light image enhancement has increasingly embraced learning-based methodologies.

**Data-driven methods.** In recent years, the rapid development of low-light image dataset collection has prompted the introduction of numerous deep learning-based enhancement methods [27]. These methods significantly improve the

restoration capabilities over traditional approaches, offering better accuracy, robustness, and speed. The first study [28], validated the effectiveness of deep learning methods in the field of low-light enhancement. [16] proposed a variant of the stacked sparse denoising autoencoder to enhance degraded images, laying a foundational framework for the application of deep learning in image enhancement. RetinexNet [19] utilized a deep Retinex-based architecture to enhance low-light images by decomposing them into illumination and reflectance components, which were processed independently. Despite its innovative approach, this method faced limitations in image decomposition, which were subsequently addressed by [29] through the development of three subnetworks based on Retinex for layer decomposition, reflectance restoration, and illumination adjustment, thereby enhancing the network's decomposition capabilities. Zero-DCE [18], FlexiCurve [30], CuDi [31], and ReLLIE [32] redefined the task of low-light enhancement as an image-specific curve estimation problem with a fixed default brightness value, notable for its rapid processing speed. RUAS [33] employed a sophisticated search unfolding technique based on a Retinex architecture. EnlightenGAN [17] innovatively utilized a generative inverse network as the main framework, initially training with unpaired images. LEDNet, introduced by [34], is a robust network specifically designed to tackle the dual challenges of low-light enhancement and deblurring simultaneously. [35] introduces PIE, a sophisticated physics-inspired contrastive learning paradigm specifically designed for enhancing low-light images. With the significant advancements of transformer models in image processing, SNRNet [20] employed a signal-to-noise ratio-aware transformer and a CNN with spatially varying operations for restoration. But it only utilizes a single global Transformer at the lowest level of the U-Net.

Totally, these methods predominantly utilize CNN models as their backbone, failing to fully leverage the emerging Transformer models that have recently gained prominence in image processing. This paper proposes a transformer model equipped with a cross-attention module, which harnesses the global perceptual capabilities of the transformer to deeply integrate the visual and semantic features extracted by CNN models.

### B. Cross Attention

In recent years, the efficacy of cross-attention modules in advanced downstream tasks has been extensively validated. In the realm of image classification, CrossVit [36] has developed a fusion module based on cross-attention that integrates tokens from both small-patch and large-patch configurations, enhancing model accuracy with minimal increases in FLOPs. In the field of multi-modal matching, [37] propose the innovative MultiModality Cross Attention (MMCA) Network for image and sentence matching. The MMCA model is adept at leveraging not only the intra-modality relationships within each modality but also the inter-modality relationships between image regions and sentence words, thereby augmenting their mutual capabilities for more effective matching. In image segmentation, [38] introduced the U-Transformer network,

which combines a U-shaped architecture with both self- and cross-attention mechanisms from the Transformer framework. In the area of few-shot classification, [39] designed a module based on cross-attention that generates cross-attention maps for each pair of class feature and query sample feature, thus highlighting the target object regions and rendering the extracted features more discriminative. In the field of few-shot object detection, TIDE [40] introduced a symmetrical cross-attention module to enhance the interaction between support features and query features, ultimately achieving notable results.

In summary, the cross-attention module has demonstrated formidable capabilities in feature fusion. Consequently, this paper embeds the cross-attention module within the Transformer block, facilitating deep integration of visual and semantic features extracted by the CNN network. By combining a multi-scale U-net network, it interacts features across different scales, ultimately achieving state-of-the-art (SOTA) performance.

### III. METHODOLOGY

In this section, we will provide a detailed description of each network module we proposed and the loss functions utilized.

Our paper proposes a transformer network with a U-shaped architecture, as illustrated in figure 1. The low light input image is first subjected to a convolutional filter to extract detailed features, obtaining semantic information and visual detail information respectively. Then, the enhanced image is obtained through the interaction enhancement of a U-shaped network using semantic- and visual-feature. The network model is optimized through VGG perceptual loss and Charbonnier L1 loss.

#### A. Problem Definition

Low light image enhancement aims to address the challenges of low brightness, low contrast, noise, and artifacts in images captured under insufficient lighting conditions. These issues stem from the loss of visual information due to inadequate illumination or complex environments when the images are taken. The goal of low light image enhancement is to restore and improve low light images  $\mathbb{L}$  through algorithms and technical methods, making them closer to normal images  $\mathbb{N}$  and more comprehensible to human visual systems.

The problem can be mathematically modeled as follows:

$$\hat{I} = f(I, \theta) \quad (1)$$

where  $I \in \mathbb{L}^{C \times H \times W}$  represents the input images,  $\hat{I} \in \mathbb{R}^{C \times H \times W}$  represents the enhanced images, and  $\theta$  represents the parameters of the network function  $f$ .

The objective of the optimization process is to find the optimal parameters  $\theta$  that minimize the differences between the enhanced images and the reference high-light images. This can be formulated as:

$$\hat{\theta} = \arg \min_{\theta} \ell(\hat{I}, R) \quad (2)$$

where  $R \in \mathbb{N}^{C \times H \times W}$  denotes the well-exposed reference images, and  $\ell$  denotes the loss function used to guide the network.

#### B. Network framework

1) *Preliminary*: Convolutional Neural Networks (CNNs) are adept at extracting detailed local features, whereas Transformer networks excel in capturing valuable global feature information from complex environments. In CNNs, as the depth of the convolutional layers increases, the extracted features progressively embody richer semantic information. Consequently, features obtained from initial shallow convolutional operations are predominantly visual in nature, while those derived from deeper convolutional layers contain more sophisticated semantic insights. To leverage these characteristics, we have designed a sophisticated convolutional extractor:

$$\begin{aligned} feat_{visual} &= Conv_1(I_{input}) \\ feat_{semantic} &= Conv_2(feat_{visual}) \end{aligned} \quad (3)$$

$feat_{visual}$  retains an abundance of detailed visual features, while  $feat_{semantic}$  preserves advanced semantic information. Both attributes are pivotal for achieving the enhanced final result.

The attention mechanism allows each element to interact with others, thereby enhancing global feature extraction capabilities significantly. The conventional self-attention mechanism is outlined as follows Eq. 4. The vectors  $Q$ ,  $K$ , and  $V$  represent query, key, and value, respectively, all derived from a single input. This operation selectively concentrates on pivotal information, optimizing resource usage and rapidly capturing the most pertinent data. Leveraging this benefit, we have developed a unique dual-branch multi head self-attention module, **DMSA**, to facilitate the fusion of two distinct features. This module processes two inputs and enables their interaction via the attention mechanism while preserving their dimensional integrity. We will provide a detailed discussion of this module in section III-B3.

$$Attention(Q, K, V) = softmax\left(\frac{QK^T}{\sqrt{d_k}}\right)V \quad (4)$$

We have integrated a U-shaped network architecture enhanced with residual connections, specifically designed to amplify the network's capability for multi-scale interaction. This architecture facilitates a comprehensive synthesis of features across different scales. In the downsampling phase, we strategically employed a  $2 \times$  scaling factor, compelling the network to engage in a rigorous compression process. This forced compression is critical as it enables the network to extract more refined global information, essential for understanding broader contextual cues. The methodology and specifics of the downsampling stage are represented in Eq. 5.

$$\begin{aligned} &[feat_{visual}, feat_{semantic}]^{(i)} = \\ Resample(DMSA\_Block_i([feat_{visual}, feat_{semantic}]^{(i-1)})) \end{aligned} \quad (5)$$

where  $\{i \in 1, 2\}$  denotes the step of the downsample stage, **DMSA\_Block** is composed of different quantities of **DMSA** modules at different steps. At the bottom of the U-shaped network, we used a bottleneck consisting of two **DMSA** modules, and during the upsampling process, we employed operations proportional to downsampling. During the upsampling phase, we incorporated residual connections to effectively preserve

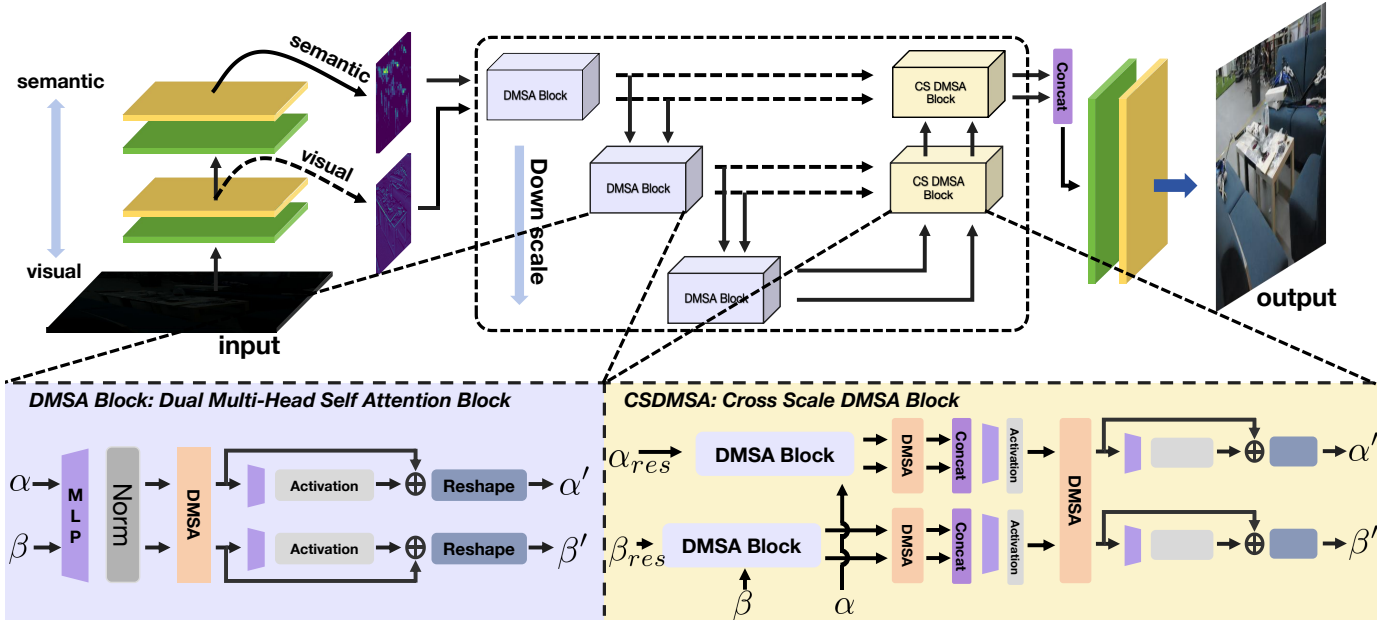


Fig. 1. The flowchart of ECAformer mainly consists of three parts: (1) Visual-Semantic convolution modules III-B2, which output short-range features (visual-feature) and long-range features (semantic-feature). (2) The U-shaped cross-attention Transformer III-B3 engages with multi-scale and multi-range input features through DMSA, concurrently propagating these features. (3) Mapping convolution, where the module projects the interacted features back to image features.  $\in \mathbb{R}^{C \times H \times W}$ .

and restore the intricate details that are often lost during the downsampling process. These residual connections first perform cross attention with their corresponding features, and then the two types of features undergo cross attention via the CSDMSA\_block. This process plays a pivotal role in maintaining the fidelity of the feature representations, ensuring that the reconstructed outputs closely mirror the original inputs. Finally, we obtain the final output through concatenation and mapping convolution. The final output can be represented by Eq. 6

$$\hat{I} = \mathcal{A}_{agg} \left( feat_{visual}^{(T)}, feat_{semantic}^{(T)} \right) \quad (6)$$



Fig. 2. From top to bottom are the shallow outputs and deep outputs of the network, respectively. It is observable that  $feat_{visual}$  focuses more on fine details, while  $feat_{semantic}$  emphasizes broader connections and contextual relationships within the image.

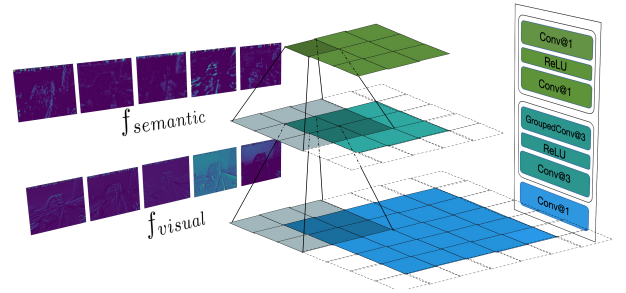


Fig. 3. Visual-Semantic Convolution Module. Deeper features focus more on semantic information, while shallower features focus more on visual information.

2) *Visual-Semantic Convolution Module*: Inspired by the potent capability of convolutional layers to enhance local features, we devised a visual-semantic convolution module specifically designed to capture local characteristics. In CNNs, as the number of convolutional layers increases, the receptive field of the model progressively enlarges, leading to the extraction of increasingly complex semantic features. However, this expansion often results in the attenuation of fine-grained detail within the features. To address this, we introduce a dedicated convolutional module that outputs two distinct types of features:  $feat_{visual}$  and  $feat_{semantic}$ . Here,  $feat_{visual}$  is derived from shallow convolution layers, capturing detailed visual features, whereas  $feat_{semantic}$  emanates from deeper convolution layers, encapsulating higher-level semantic information. Additionally, convolutional neural networks are inherently capable of capturing periodic and local spatial features, addressing the spatial context induction bias in transformers that rely solely on positional embeddings. We employ depth-

wise separable convolution within this module to enhance the rate of forward propagation without compromising accuracy. Upon processing through this module, the network then employs attention mechanisms to facilitate a dynamic interaction between these two distinct features.

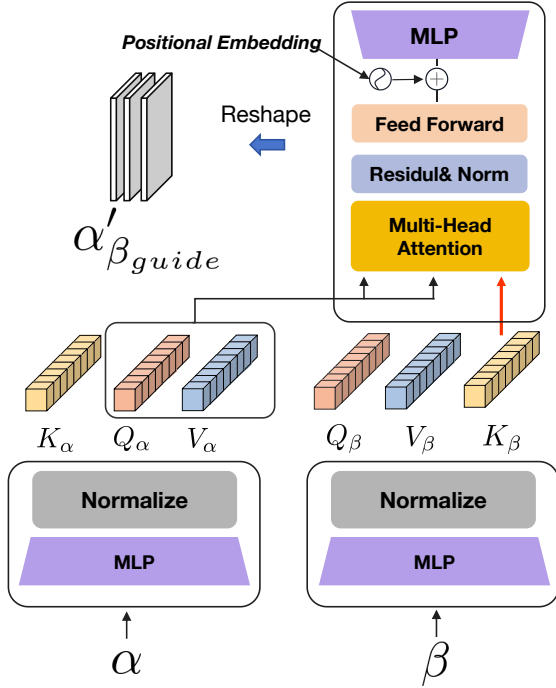


Fig. 4. DMSA: A highly symmetrical module is depicted in the figure, which illustrates the process of computing the  $\alpha$  features guided by  $\beta$  ( $\alpha_{\beta_{guided}}$ ). The  $\beta_{\alpha_{guided}}$  can be obtained through a symmetrical approach.

3) *DMSA*: Self-attention is highly efficient at directing concentrated attention towards pivotal information, thereby optimizing resource utilization and rapidly acquiring the most relevant data. However, its standard configuration is restricted to processing only a single input, which can limit its applicability in scenarios requiring complex interactions between multiple data streams. To address this constraint, we have innovated the Dual Multi-head Self Attention (**DMSA**) module, a sophisticated mechanism designed to effectively manage and integrate dual inputs. In this module, inputs  $\alpha$  and  $\beta$  are processed to generate distinct sets of  $Q$ ,  $K$ , and  $V$  vectors through separate mappings. We strategically cross the key vectors of both inputs within this module to enhance their interconnectivity, fostering a richer, more comprehensive interaction. This is achieved by the multiplication of the query vector with the corresponding crossed key vector, producing an attention map that encapsulates the intricate dynamics between the two inputs. Enhanced by the adaptive sampling operations of the U-shaped network, this setup facilitates a profound interaction across multiple scales, allowing for a nuanced integration of features that is essential for complex analysis and interpretation tasks.

$$DMSA(Q_{\alpha}, K_{\beta}, V_{\alpha}) = softmax(Q_{\alpha}K_{\beta}^T * \zeta_{rescale})V_{\alpha} \quad (7)$$

The scaling factor  $\zeta_{rescale}$  is determined through optimization. To preserve the spatial positional relationships among pixels, we have incorporated a position encoding module, executed via convolutional operations. Consequently, the output of the Dual Multi-head Self Attention module can be formally defined in Eq. 8.

$$[\alpha', \beta'] = [DMSA(Q_{\alpha}, K_{\beta}, V_{\alpha}) + PosEmbed(V_{\alpha}), DMSA(Q_{\beta}, K_{\alpha}, V_{\beta}) + PosEmbed(V_{\beta})] \quad (8)$$

### C. Loss function

We incorporated two types of loss functions that better align with human visual perception and facilitate faster model training. TotalLoss can be represented as Eq. 9,  $\lambda \in [0, 1]$ .

$$TotalLoss = \lambda * \mathcal{L}_p + (1 - \lambda) * \mathcal{L}_c \quad (9)$$

where  $\mathcal{L}_p$  is the loss of perceptual and  $\mathcal{L}_c$  is the loss of charbonnier.

1) *Perceptual Loss*: Perceptual Loss [41] adopts a efficient approach by quantifying the discrepancies through the squared error between features extracted from specific layers or an aggregation of multiple layers after both the ground truth and the reconstructed image have traversed the same pre-trained neural network. This technique transcends traditional pixel-based difference calculations, offering a superior method for handling anomalies and enhancing the overall robustness of the model. By focusing the loss calculations on the variances within the deeper layers of feature representations, Perceptual Loss adeptly captures and emphasizes high-level semantic nuances. Consequently, this approach produces images that more accurately reflect human visual perceptions, thereby aligning the output more closely with the intricacies of human sight.

$$PerceptualLoss = \sum_{i=1}^n \frac{1}{C_i H_i W_i} |F_i^l(f(\hat{I})) - F_i^l(R)|^2 \quad (10)$$

Among them,  $f$  symbolizes the enhancement network.  $F_i^l$  indicates the  $i$ -th feature map in the  $l$ -th layer. We have utilized a VGG-19 network pre-trained on ImageNet and employed the output feature maps from its initial five ReLU layers to compute the loss. This method leverages the deep network's architecture to extract rich, complex feature representations that are critical for assessing the perceptual quality of the enhanced images.

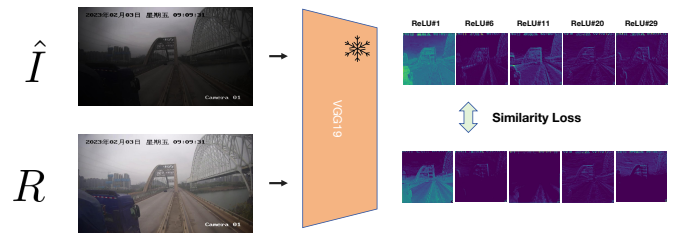


Fig. 5. Perceptual Loss: Implementing loss on the features extracted from a frozen VGG19 network

2) *Charbonnier  $L_1$  Loss*: Compared to the conventional  $L_1$  Loss, Charbonnier  $L_1$  Loss exhibits superior robustness and stability, particularly when dealing with outliers. Additionally, the computational efficiency of Charbonnier  $L_1$  Loss is enhanced due to its reliance on a single square and root operation, in contrast to the ordinary  $L_1$  Loss which necessitates an absolute value computation. This streamlined calculation not only speeds up the processing but also contributes to smoother gradients, facilitating more effective optimization during model training.

$$\text{CharbonnierLoss} = \sum_{i=1}^n \sqrt{(\hat{I} - R)^2 + \epsilon^2} \quad (11)$$

Benefiting from the addition of epsilon, the phenomenon of gradient vanishing when  $\hat{I}$  and  $R$  are very close has been alleviated, making the model easier to train.

#### IV. EXPERIMENT

##### A. Experimental configurations

**Datasets.** We conducted comparisons across multiple public datasets: LOL-v1 [19], LOL-v2 [42], SID [43], SMID [44], and SDDS [45].

*Traffic-297.* We have gathered 297 images captured by traffic video cameras and, following the LOL methodology, have created corresponding image pairs. These images encompass diverse weather conditions and traffic scenarios. Among them, 50 images are dedicated for testing purposes, while 247 are allocated for training.

*LOL-v1.* It represents the inaugural dataset comprising paired low- and normal-light images captured in real-world scenarios. The low-light images within this collection are meticulously gathered by adjusting exposure times and ISO settings. The dataset encompasses 500 pairs of low- and normal-light images, each with dimensions of 400×600 and preserved in RGB format, offering a comprehensive resource for enhancing low-light image processing techniques. The training and testing sets are split in proportion to 485:15.

*LOL-v2.* The LOL-v2 dataset consists of two distinct subsets: LOL-v2-real and LOL-v2-synthetic. The LOL-v2-real subset is captured in real scenes by altering ISO settings and exposure times. In the LOL-v2-synthetic subset, low-light images are synthesized from RAW images by analyzing the illumination distribution in low-light conditions. The training and testing sets are split in proportion to 689:100 and 900:100.

*SID.* The Sony  $\alpha 7S$  II subset of the SID dataset is utilized for evaluation purposes. It consists of 2,697 pairs of short/long-exposure RAW images. The low-/normal-light RGB images are derived by applying the SID’s in-camera signal processing techniques to convert RAW images to RGB format. Of these, 2,099 image pairs are designated for training, while 598 pairs are reserved for testing.

*SMID.* The SMID benchmark amasses a collection of 20,809 short-/long-exposure RAW image pairs. We convert these RAW datasets into low-/normal-light RGB image pairs, utilizing a consistent transformation process to ensure data integrity. For model training, 15,763 pairs are utilized, while the remaining pairs are set aside for rigorous testing.

TABLE I  
RESULTS ON TRAFFIC-297

	RetinexNet	ZeroDCE++	EnGAN	SNR	ECAFormer
PSNR	18.56	18.35	18.19	30.06	<u>32.17</u>
SSIM	0.77	0.884	0.623	0.965	<u>0.975</u>

*SDDS.* We utilize the static version of the SDDS dataset, which was captured using a Canon EOS 6D Mark II camera equipped with an ND filter. The dataset comprises both indoor and outdoor subsets. For the SDDS-indoor subset, we allocate 62 low-/normal-light video pairs for training and 6 pairs for testing. Similarly, for the SDDS-outdoor subset, 116 pairs are used for training while 10 pairs are reserved for testing.

**Training.** We implemented the ECAFormer model using PyTorch. The model was trained on an NVIDIA RTX 4090 with 24 GB of VRAM using the Adam optimizer ( $\beta_1 = 0.9$  and  $\beta_2 = 0.999$ ), across a total of 250,000 iterations. The initial learning rate was set at  $2 \times 10^{-4}$  and gradually reduced to  $1 \times 10^{-6}$  through a cosine annealing schedule during the training process. Training samples were generated by randomly cropping 128×128 patches from pairs of low-/normal-light images. The batch size was set to 8. The training data was augmented with random rotations and flips to enhance variability and robustness. The training objective was to minimize both *PerceptualLossIII-C1* and *Charbonnier  $L_1$  LossIII-C2* between the enhanced images and their corresponding ground truths, ensuring high fidelity in the restoration of image details and color accuracy.

**Metrics.** We employ the peak signal-to-noise ratio (PSNR) Eq. 12 and structural similarity index (SSIM) Eq. [46]13 as the primary metrics for evaluation.

$$\text{PSNR} = 10 \cdot \log_{10} \left( \frac{\text{MAX}_I^2}{\text{MSE}} \right) \quad (12)$$

$$\text{SSIM}(x, y) = \frac{(2\mu_x\mu_y + c_1)(2\sigma_{xy} + c_2)}{(\mu_x^2 + \mu_y^2 + c_1)(\sigma_x^2 + \sigma_y^2 + c_2)} \quad (13)$$

**Comparison Methods.** To validate the effectiveness of the model, we conducted extensive comparisons with state-of-the-art models in recent years. The compared models are as follows: SID [43], UFormer(UF) [47], RetinexNet(RN) [19], EnlightenGAN(EnGAN) [17], RUAS [33], DRBN [48], KinD [29], Restormer [49], MIRNet [50], SNR-Net [20].

##### B. Results analysis

**Quantitative Results.** We compared our model across seven public datasets using two metrics, PSNR and SSIM, with the results presented respectively in Table III and Table IV. The results indicate that our model achieves state-of-the-art (SOTA) performance while maintaining a relatively low parameter count and computational complexity.

**Quality Results.** In Figures IV-B and 8, we present visual comparison charts of the results. The recent fully supervised learning method, SNR, did not retain sufficient detail and exhibited blurring. ZeroDCE++, which adjusts the pixel curves, introduced excessive noise. The results demonstrate that the

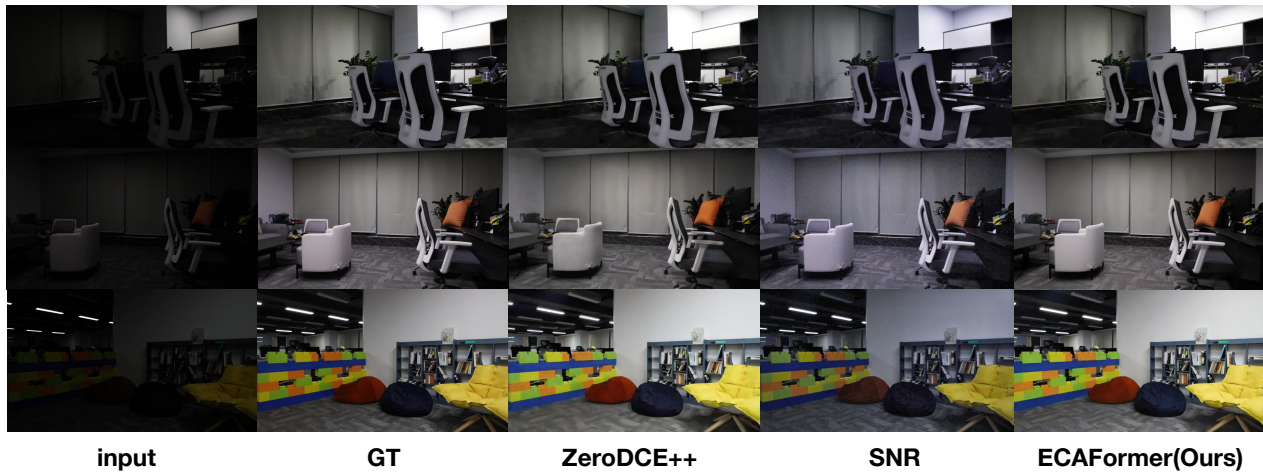


Fig. 6. Comparative Visual Effects on the Test Set

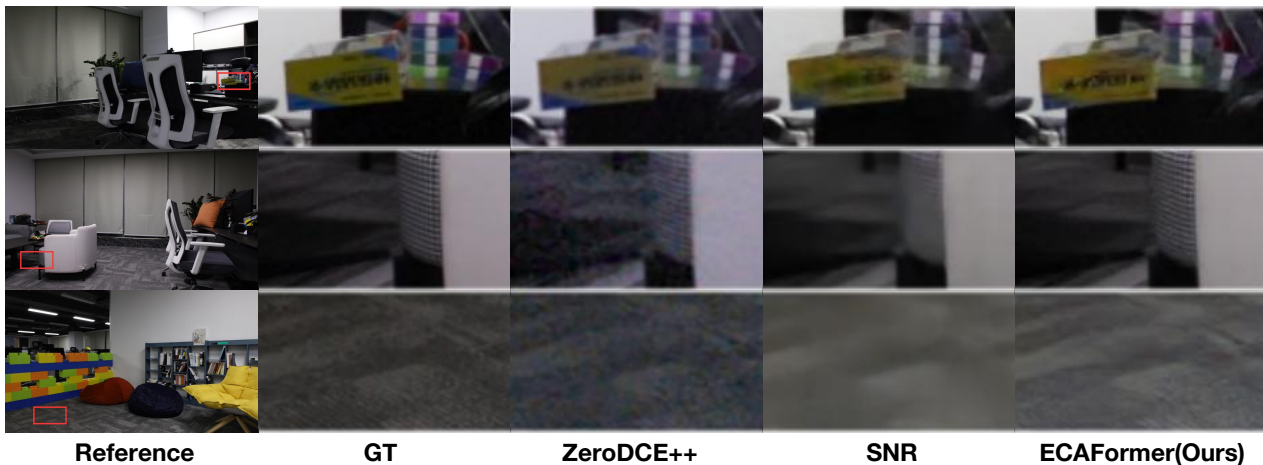


Fig. 7. Visual Detail Comparison on the Test Set

ECAFormer proposed in this paper produces high-quality outcomes that closely approximate the true images.

### C. Ablation study

To validate the effectiveness of the various modules within the model proposed in this article, we adjusted the model’s structure and reported the PSNR results on the SDSO-out dataset.

**CNN\_feat.** We validated the effectiveness of the shallow-deep convolution module. When this module is not utilized, the input image is directly reshaped to the format required by the MGMSA for input.

**VGG\_CbLoss.** Verified the effectiveness of the loss functions by comparing the Mean Squared Error (MSE) loss with the two types of losses used in this study.

**DMSA.** Replaced the DMSA with a classic self-attention mechanism to validate the performance of this module in feature fusion.

The results indicate that all three modules positively impact the model’s performance and are effective. Among them, the

TABLE II  
ABLATION STUDY RESULTS ON SDSO-OUT

CNN_feat	VGG_CbLoss	DMSA	PSNR(avg)
	✓	✓	28.56
✓		✓	29.41
✓	✓		28.38
✓	✓	✓	29.57

DMSA module demonstrates the most significant performance in terms of feature fusion.

## V. CONCLUSION

In this paper, we propose a one-stage transformer-based method, specifically utilizing DMSA blocks for enhancing low-light images. Furthermore, the network of **ECAFormer** combines the benefits of the local detailed feature information extraction ability in Convolutional Neural Network and global information extraction ability in the Transformer Network. Therefore, **ECAFormer** can extract global information and local information from the image. Extensive experiment



Fig. 8. Visual Detail Comparison on the Traffic-297. We tested models trained on the synthesised dataset under real-world nighttime scenarios. While other methods introduce noise and lose details, our model exhibits excellent visual performance.

TABLE III  
COMPARISON OF PSNR ACROSS EIGHT PUBLIC DATASETS USING DIFFERENT METHODS. ECAFORMER ACHIEVED PROMISING RESULTS WITH THE LEAST NUMBER OF PARAMETERS.

	SID	UF	RN	EnGAN	RUAS	DRBN	KinD	RSTM	MIRNet	SNR	ECA
LOL-v1	14.35	16.36	16.77	17.48	18.23	20.13	20.86	22.43	24.14	<u>24.61</u>	24.24
LOL-v2-r	13.24	18.82	15.47	18.23	18.37	20.29	14.74	19.94	20.02	21.48	21.99
LOL-v2-s	15.04	19.66	17.13	16.57	16.55	23.22	13.29	21.41	21.94	24.14	<u>25.86</u>
SID	16.97	18.54	16.48	17.23	18.44	19.02	18.02	22.27	20.84	22.87	24.69
SMID	24.78	27.2	22.83	22.62	25.88	26.6	22.18	26.97	25.66	28.49	<u>29.34</u>
SDSD-in	23.29	23.17	20.84	20.02	23.17	24.08	21.95	25.67	24.38	29.44	29.11
SDSD-out	24.9	23.85	20.96	20.1	23.84	25.77	21.97	24.79	27.13	28.66	<u>29.57</u>
FLOPS	13.73	12	587.47	61.01	0.83	48.61	34.99	144.25	785	26.35	27.34
Params	7.76	5.29	0.84	114.35	0.003	5.27	8.02	26.13	31.76	4.01	2.5

TABLE IV  
COMPARISON OF SSIM ACROSS EIGHT PUBLIC DATASETS USING DIFFERENT METHODS

	SID	UF	RN	EnGAN	RUAS	DRBN	KinD	RSTM	MIRNet	SNR	ECA
LOL-v1	0.436	0.771	0.56	0.65	0.72	0.83	0.79	0.823	0.83	0.842	<u>0.85</u>
LOL-v2-r	0.442	0.771	0.567	0.617	0.723	0.831	0.641	0.827	0.82	0.849	<u>0.853</u>
LOL-v2-s	0.61	0.871	0.798	0.734	0.652	0.927	0.578	0.83	0.876	0.928	<u>0.931</u>
SID	0.591	0.577	0.578	0.543	0.581	0.577	0.583	0.649	0.605	0.625	<u>0.66</u>
SMID	0.718	0.792	0.684	0.674	0.744	0.781	0.634	0.758	0.762	0.805	<u>0.81</u>
SDSD-in	0.703	0.859	0.617	0.604	0.696	0.868	0.672	0.827	0.864	0.894	0.874
SDSD-out	0.693	0.748	0.629	0.616	0.743	0.841	0.654	0.802	0.837	<u>0.866</u>	0.862

results verify the competitive advantages of **ECAFormer** compared with other state-of-the-art algorithms.

**Future work.** In recent years, models trained on extensive datasets have progressively evolved. The integration of prior knowledge from large models can mitigate the limitations of current loss functions and extend to unsupervised learning. The two-dimensional Fourier transform holds substantial potential in handling image details and could be incorporated into the DMSA module proposed in this paper, enabling interactions in both the frequency and time domains.

REFERENCES

- [1] B. Ranft and C. Stiller, “The role of machine vision for intelligent vehicles,” *IEEE Transactions on Intelligent vehicles*, vol. 1, no. 1, pp. 8–19, 2016.
- [2] P. Cai, Y. Sun, H. Wang, and M. Liu, “Vtgnnet: A vision-based trajectory generation network for autonomous vehicles in urban environments,” *IEEE Transactions on Intelligent Vehicles*, vol. 6, no. 3, pp. 419–429, 2020.
- [3] G. Bresson, Z. Alsayed, L. Yu, and S. Glaser, “Simultaneous localization and mapping: A survey of current trends in autonomous driving,” *IEEE Transactions on Intelligent Vehicles*, vol. 2, no. 3, pp. 194–220, 2017.
- [4] L. Fu, H. Yu, F. Juefei-Xu, J. Li, Q. Guo, and S. Wang, “Let there be light: Improved traffic surveillance via detail preserving night-to-day transfer,” *IEEE Transactions on Circuits and Systems for Video Technology*, vol. 32, no. 12, pp. 8217–8226, 2021.



- [5] M. Zhao, Y. Zhou, X. Li, W. Cao, C. He, B. Yu, X. Li, C. D. Elvidge, W. Cheng, and C. Zhou, "Applications of satellite remote sensing of nighttime light observations: Advances, challenges, and perspectives," *Remote Sensing*, vol. 11, no. 17, p. 1971, 2019.
- [6] H. Ibrahim and N. S. P. Kong, "Brightness preserving dynamic histogram equalization for image contrast enhancement," *IEEE Transactions on Consumer Electronics*, vol. 53, no. 4, pp. 1752–1758, 2007.
- [7] M. Abdullah-Al-Wadud, M. H. Kabir, M. A. A. Dewan, and O. Chae, "A dynamic histogram equalization for image contrast enhancement," *IEEE transactions on consumer electronics*, vol. 53, no. 2, pp. 593–600, 2007.
- [8] X. Fu, Y. Liao, D. Zeng, Y. Huang, X.-P. Zhang, and X. Ding, "A probabilistic method for image enhancement with simultaneous illumination and reflectance estimation," *IEEE Transactions on Image Processing*, vol. 24, no. 12, pp. 4965–4977, 2015.
- [9] Z. Gu, F. Li, F. Fang, and G. Zhang, "A novel retinex-based fractional-order variational model for images with severely low light," *IEEE Transactions on Image Processing*, vol. 29, pp. 3239–3253, 2019.
- [10] S. Hao, X. Han, Y. Guo, X. Xu, and M. Wang, "Low-light image enhancement with semi-decoupled decomposition," *IEEE transactions on multimedia*, vol. 22, no. 12, pp. 3025–3038, 2020.
- [11] X. Guo, Y. Li, and H. Ling, "Lime: Low-light image enhancement via illumination map estimation," *IEEE Transactions on image processing*, vol. 26, no. 2, pp. 982–993, 2016.
- [12] M. Li, J. Liu, W. Yang, X. Sun, and Z. Guo, "Structure-revealing low-light image enhancement via robust retinex model," *IEEE Transactions on Image Processing*, vol. 27, no. 6, pp. 2828–2841, 2018.
- [13] S. Wang, J. Zheng, H.-M. Hu, and B. Li, "Naturalness preserved enhancement algorithm for non-uniform illumination images," *IEEE transactions on image processing*, vol. 22, no. 9, pp. 3538–3548, 2013.
- [14] S. Park, S. Yu, B. Moon, S. Ko, and J. Paik, "Low-light image enhancement using variational optimization-based retinex model," *IEEE Transactions on Consumer Electronics*, vol. 63, no. 2, pp. 178–184, 2017.
- [15] X. Ren, W. Yang, W.-H. Cheng, and J. Liu, "Lr3m: Robust low-light enhancement via low-rank regularized retinex model," *IEEE Transactions on Image Processing*, vol. 29, pp. 5862–5876, 2020.
- [16] K. G. Lore, A. Akintayo, and S. Sarkar, "Llnet: A deep autoencoder approach to natural low-light image enhancement," *Pattern Recognition*, vol. 61, pp. 650–662, 2017.
- [17] Y. Jiang, X. Gong, D. Liu, Y. Cheng, C. Fang, X. Shen, J. Yang, P. Zhou, and Z. Wang, "Enlightengan: Deep light enhancement without paired supervision," *IEEE transactions on image processing*, vol. 30, pp. 2340–2349, 2021.
- [18] C. Guo, C. Li, J. Guo, C. C. Loy, J. Hou, S. Kwong, and R. Cong, "Zero-reference deep curve estimation for low-light image enhancement," in *Proceedings of the IEEE/CVF conference on computer vision and pattern recognition*, 2020, pp. 1780–1789.
- [19] C. Wei, W. Wang, W. Yang, and J. Liu, "Deep retinex decomposition for low-light enhancement," *arXiv preprint arXiv:1808.04560*, 2018.
- [20] X. Xu, R. Wang, C.-W. Fu, and J. Jia, "Snr-aware low-light image enhancement," in *Proceedings of the IEEE/CVF conference on computer vision and pattern recognition*, 2022, pp. 17 714–17 724.
- [21] S. M. Pizer, "Contrast-limited adaptive histogram equalization: Speed and effectiveness stephen m. pizer, r. eugene johnston, james p. ericksen, bonnie c. yankaskas, keith e. muller medical image display research group," in *Proceedings of the first conference on visualization in biomedical computing, Atlanta, Georgia*, vol. 337, 1990, p. 1.
- [22] J. A. Stark, "Adaptive image contrast enhancement using generalizations of histogram equalization," *IEEE Transactions on image processing*, vol. 9, no. 5, pp. 889–896, 2000.
- [23] T. Arici, S. Dikbas, and Y. Altunbasak, "A histogram modification framework and its application for image contrast enhancement," *IEEE Transactions on image processing*, vol. 18, no. 9, pp. 1921–1935, 2009.
- [24] E. H. Land, "The retinex theory of color vision," *Scientific american*, vol. 237, no. 6, pp. 108–129, 1977.
- [25] D. J. Jobson, Z.-u. Rahman, and G. A. Woodell, "A multiscale retinex for bridging the gap between color images and the human observation of scenes," *IEEE Transactions on Image processing*, vol. 6, no. 7, pp. 965–976, 1997.
- [26] S. Rahman, M. M. Rahman, M. Abdullah-Al-Wadud, G. D. Al-Quaderi, and M. Shoyaib, "An adaptive gamma correction for image enhancement," *EURASIP Journal on Image and Video Processing*, vol. 2016, pp. 1–13, 2016.
- [27] C. Li, C. Guo, L. Han, J. Jiang, M.-M. Cheng, J. Gu, and C. C. Loy, "Low-light image and video enhancement using deep learning: A survey," *IEEE transactions on pattern analysis and machine intelligence*, vol. 44, no. 12, pp. 9396–9416, 2021.
- [28] H. Jiang and Y. Zheng, "Learning to see moving objects in the dark," in *2019 IEEE/CVF International Conference on Computer Vision (ICCV)*, 2019, pp. 7323–7332.
- [29] Y. Zhang, J. Zhang, and X. Guo, "Kindling the darkness: A practical low-light image enhancer," in *Proceedings of the 27th ACM international conference on multimedia*, 2019, pp. 1632–1640.
- [30] C. Li, C. Guo, S. Zhou, Q. Ai, R. Feng, and C. C. Loy, "Flexicurve: Flexible piecewise curves estimation for photo retouching," in *Proceedings of the IEEE/CVF Conference on Computer Vision and Pattern Recognition*, 2023, pp. 1092–1101.
- [31] C. Li, C. Guo, R. Feng, S. Zhou, and C. C. Loy, "Cudi: Curve distillation for efficient and controllable exposure adjustment," 2022.
- [32] R. Zhang, L. Guo, S. Huang, and B. Wen, "Reliie: Deep reinforcement learning for customized low-light image enhancement," *arXiv preprint arXiv:2107.05830*, 2021.
- [33] R. Liu, L. Ma, J. Zhang, X. Fan, and Z. Luo, "Retinex-inspired unrolling with cooperative prior architecture search for low-light image enhancement," in *Proceedings of the IEEE/CVF conference on computer vision and pattern recognition*, 2021, pp. 10 561–10 570.
- [34] S. Zhou, C. Li, and C. C. Loy, "Lednet: Joint low-light enhancement and deblurring in the dark," 2022.
- [35] D. Liang, Z. Xu, L. Li, M. Wei, and S. Chen, "Pie: Physics-inspired low-light enhancement," 2024.
- [36] C.-F. R. Chen, Q. Fan, and R. Panda, "Crossvit: Cross-attention multi-scale vision transformer for image classification," in *Proceedings of the IEEE/CVF International Conference on Computer Vision (ICCV)*, October 2021, pp. 357–366.
- [37] X. Wei, T. Zhang, Y. Li, Y. Zhang, and F. Wu, "Multi-modality cross attention network for image and sentence matching," in *Proceedings of the IEEE/CVF Conference on Computer Vision and Pattern Recognition (CVPR)*, June 2020.
- [38] O. Petit, N. Thome, C. Rambour, L. Themyr, T. Collins, and L. Soler, "U-net transformer: Self and cross attention for medical image segmentation," in *Machine Learning in Medical Imaging: 12th International Workshop, MLMI 2021, Held in Conjunction with MICCAI 2021, Strasbourg, France, September 27, 2021, Proceedings 12*. Springer, 2021, pp. 267–276.
- [39] R. Hou, H. Chang, B. Ma, S. Shan, and X. Chen, "Cross attention network for few-shot classification," 2019.
- [40] W. Li, H. Wei, Y. Wu, J. Yang, Y. Ruan, Y. Li, and Y. Tang, "Tide: Test-time few-shot object detection," *IEEE Transactions on Systems, Man, and Cybernetics: Systems*, pp. 1–10, 2024.
- [41] J. Johnson, A. Alahi, and L. Fei-Fei, "Perceptual losses for real-time style transfer and super-resolution," in *Computer Vision—ECCV 2016: 14th European Conference, Amsterdam, The Netherlands, October 11–14, 2016, Proceedings, Part II 14*. Springer, 2016, pp. 694–711.
- [42] W. Yang, W. Wang, H. Huang, S. Wang, and J. Liu, "Sparse gradient regularized deep retinex network for robust low-light image enhancement," *IEEE Transactions on Image Processing*, vol. 30, pp. 2072–2086, 2021.
- [43] C. Chen, Q. Chen, M. N. Do, and V. Koltun, "Seeing motion in the dark," in *Proceedings of the IEEE/CVF International conference on computer vision*, 2019, pp. 3185–3194.
- [44] C. Chen, Q. Chen, J. Xu, and V. Koltun, "Learning to see in the dark," in *Proceedings of the IEEE conference on computer vision and pattern recognition*, 2018, pp. 3291–3300.
- [45] R. Wang, X. Xu, C.-W. Fu, J. Lu, B. Yu, and J. Jia, "Seeing dynamic scene in the dark: A high-quality video dataset with mechatronic alignment," in *Proceedings of the IEEE/CVF International Conference on Computer Vision*, 2021, pp. 9700–9709.
- [46] Z. Wang, A. Bovik, H. Sheikh, and E. Simoncelli, "Image quality assessment: from error visibility to structural similarity," *IEEE Transactions on Image Processing*, vol. 13, no. 4, pp. 600–612, 2004.
- [47] Z. Wang, X. Cun, J. Bao, W. Zhou, J. Liu, and H. U. Li, "A general u-shaped transformer for image restoration. arxiv 2021," *arXiv preprint arXiv:2106.03106*.
- [48] W. Yang, S. Wang, Y. Fang, Y. Wang, and J. Liu, "Band representation-based semi-supervised low-light image enhancement: Bridging the gap between signal fidelity and perceptual quality," *IEEE Transactions on Image Processing*, vol. 30, pp. 3461–3473, 2021.
- [49] S. W. Zamir, A. Arora, S. Khan, M. Hayat, F. S. Khan, and M.-H. Yang, "Restormer: Efficient transformer for high-resolution image restoration," in *Proceedings of the IEEE/CVF conference on computer vision and pattern recognition*, 2022, pp. 5728–5739.
- [50] S. W. Zamir, A. Arora, S. Khan, M. Hayat, F. S. Khan, M.-H. Yang, and L. Shao, "Learning enriched features for real image restoration and enhancement," in *Computer Vision—ECCV 2020: 16th European*

*Conference, Glasgow, UK, August 23–28, 2020, Proceedings, Part XXV*  
16. Springer, 2020, pp. 492–511.